Thin Solid Films 674 (2019) 64–70

Contents lists available at ScienceDirect

Thin Solid Films

journal homepage: www.elsevier.com/locate/tsf

Properties of tungsten thin film deposited using inductively coupled plasma assisted sputtering for next-generation interconnect metal

Soo Jung Lee[a], Tae Hyung Kim[a], Byeong-Hwa Jeong[a], Kyong Nam Kim[c], Geun Young Yeom[a,b,*]

[a] Department of Materials Science and Engineering, Sungkyunkwan University, Suwon, Gyeonggi-Do 440-746, South Korea
[b] SKKU Advanced Institute of Nano Technology (SAINT), Sungkyunkwan University, Suwon, Gyeonggi-Do 440-746, South Korea
[c] Department of Advanced Materials, Daejeon University, 62 Daehak-ro, Dong-gu, Daejeon 300-716, Republic of Korea

ABSTRACT

Tungsten (W) is actively investigated as one of the future metallization materials which can replace Cu for the metal thickness lower than tens of nanometer due to its sfmall electron mean free path of 19 nm and high melting temperature of 3673 K. In this study, inductively coupled plasma (ICP) assisted DC magnetron sputtering of W has been investigated for the lower resistivity of nm scale W film (30 nm). When the characteristics of W thin films deposited with and without ICP assistance were investigated, the decrease of the W thin film resistivity with the increase of deposition rate was observed as the ICP power is increased regardless of substrate heating. The decrease of W thin film resistivity by the ICP assisted DC sputter deposition was related to the change of crystal structure from A-15 to BCC, decreased oxygen incorporation in the film, decreased surface roughness, and increased grain size due to the increased ion flux to the substrate.

1. Introduction

As the critical dimensions of the semiconductor devices are reduced under 10 nm due to the high integration of semiconductor devices, the characteristics of the metallization have become one of the factors that greatly affect the performance and reliability of semiconductor devices such as dynamic random access memory and 3D NAND (Not And) devices. The resistivity is significantly increased due to the decrease of the device width, and the transmission delay (resistor-capacitor delay) with the increase of the resistivity limits the speed of the device. In addition, the decrease in the cross-sectional area of the interconnection increased the current densities and stress of the interconnection, thereby, lowering the reliability of the metal interconnection.

Copper (Cu) has a high conductivity, and it is the most commonly used as a metallization. However, there are limitations in using Cu as the metallization for the critical dimension lower than tens of nanometer; the resistivity of Cu increases sharply due to the size effect linked to the long electron mean free path (EMFP) of 39 nm [1–7] and the reliability of Cu is degraded as the device operating temperatures and current densities increase with each technology node [8,9]. The reliability of Cu metallization is also hurdles for advanced technology nodes, such as 10 nm node [10]. Because of these limitations, researches on the next generation interconnection materials have been actively conducted [11].

From a few decades ago, studies have been reported replacing Cu with W in the back end of interconnection process, which is one of the semiconductor device fabrication processes because of its smaller EMFP of 19 nm and very high melting point (3695 K compared with Cu of 1357 K) [2,3,8,12,13]. Since W has a smaller EMFP than Cu, it is expected to reduce the size effect of surface scattering and grain boundary scattering mechanism as expected by MS model and FS model as it goes to nanometer dimension [3,14].

The methods for depositing materials such as chemical deposition, atomic layer deposition, and sputter deposition have been widely used during a few decades. Among these, sputter deposition has been used for manufacturing semiconductor and thin film transistor due to high and uniform deposition rate at low temperatures [15,16]. It is suitable for use in industry and laboratories due to the high quality of the deposited materials, the high deposition rate, and the versatility of the materials to be deposited [17,18]. Especially nowadays, variously modified sputter deposition technology such as pulse modulated sputter deposition, plasma assisted sputter deposition, bias sputtering, remote ion beam assisted sputter deposition, etc. has been widely investigated for depositing thin films. These methods were used to improve the film quality by enhancing the surface diffusion on the substrate through the density and/or energy of the ions bombarding the substrate [19,20]. For example, the bias sputtering has been applied to improve the quality films close to the bulk materials by controlling the ion energy bombarding the substrate [21,22]. Remote ion beam assisted sputter deposition methods were studied to control the nucleation and growth of thin film by varying not only the ion energy but also the angle of ion bombardment using a separate remote type ion gun [23–26]. Plasma

* Corresponding author.
E-mail address: gyyeom@skku.edu (G.Y. Yeom).

https://doi.org/10.1016/j.tsf.2019.01.051
Received 31 August 2018; Received in revised form 29 January 2019; Accepted 29 January 2019
Available online 30 January 2019
0040-6090/

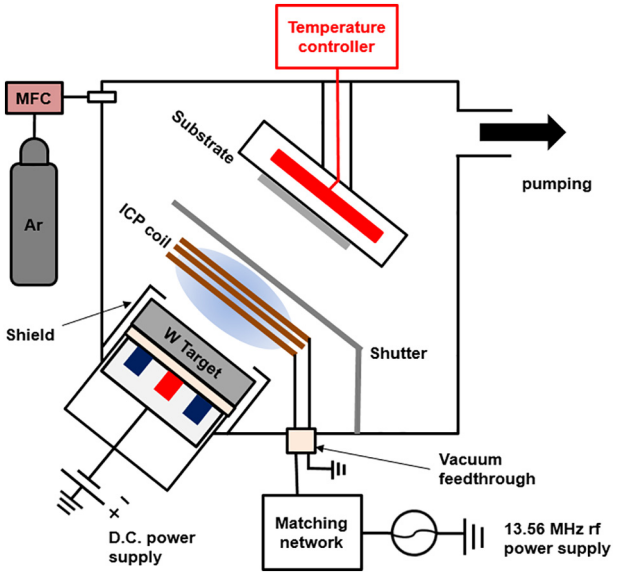

Fig. 1. Schematic diagram of the ICP assisted DC power magnetron sputter system used for depositing W film.

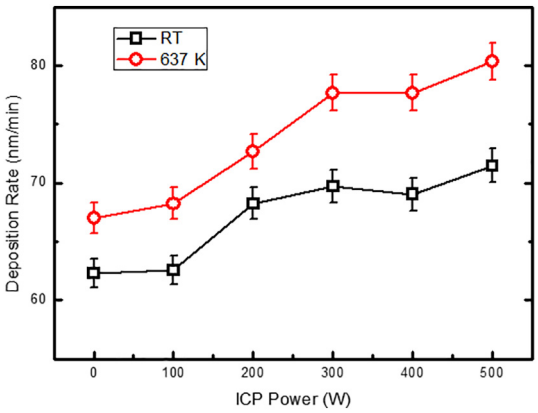

Fig. 2. Deposition rate of W film as a function of ICP power (from 0 to 500 W) for two different substrate temperatures (RT and 673 K).

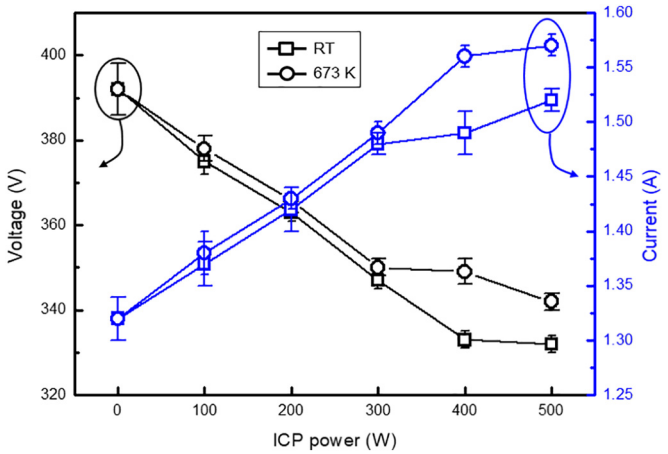

Fig. 3. Variation of voltage and current of DC magnetron sputter magnetron as a function of ICP power (from 0 W to 500 W) while maintaining the DC magnetron power of 500 W at 2.0 Pa Ar for different substrate temperatures (RT and 673 K).

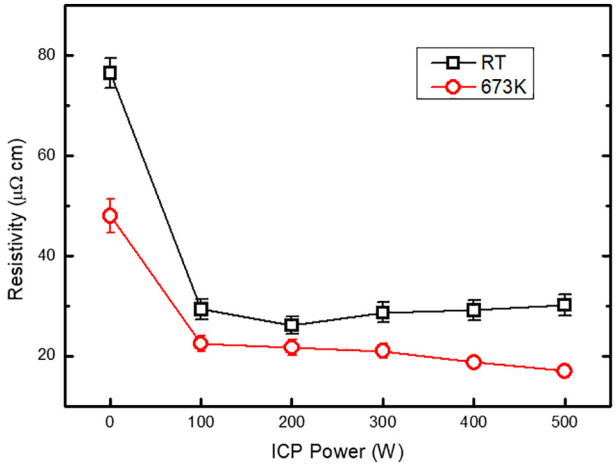

Fig. 4. Resistivity of the deposited W film as a function of ICP power for different substrate temperatures of RT and 673 K while maintaining the DC power of 500 W at 2.0 Pa Ar. The thickness of W thin films was 30 nm.

assisted sputter deposition methods such as inductively coupled plasma (ICP) assisted sputter deposition methods have been also investigated to increase the ion density significantly while decreasing the ion bombardment energy to the substrate for the control of the nucleation and growth of depositing thin film, therefore, to improve the electrical properties of deposited W films such as electron mobility and conductivity [27–29].

In this study, W metallization was studied to investigate the possibility of substitution of Cu metallization. ICP assisted sputtering with no bias to the substrate has been investigated to decrease the resistivity of nanometer scale W film. A conventional DC magnetron sputter system with an internal-type coil antenna for the ICP source has been used. By using the ICP assisted DC sputtering, improved material characteristics of the film, therefore, lower W thin film resistivity could be obtained. As a result, the feasibility of W deposited by ICP assisted sputtering as a next-generation metallization material could be investigated.

2. Experimental

Fig. 1 shows the schematic diagram of the ICP assisted DC magnetron sputtering system. The size of the magnetron target was 3 in. diameter, and the ICP coil was located above the target. The ICP coil consists of one-turn oxygen-free copper tube of 6.35 mm diameter. The base pressure was maintained $< 1.33 \times 10^{-4}$ Pa by pumping using a turbomolecular pump (OSAKA VACUUM - TH520). A DC power supply (ENI, RPG-100) was connected to the magnetron sputter target, and 13.56 MHz RF power (ADVANCED ENERGY, RFX-600) was applied to the ICP coil and was connected after passing through a matching network for impedance matching. The spacing between the target and the substrate with the area of 50 mm × 50 mm was 70 mm.

The sputtering was carried out with Ar (30 sccm) and at 2.0 Pa of operating pressure. DC power was fixed at 500 W and the RF power the ICP coil was varied from 0 to 500 W. The SiO_2 wafer was used for the substrate and, before the deposition on the substrate, the sputter target was pre-sputtered for 2 min to clean the target surface. As the sputter target, 3 in. diameter 99.999% pure W target was used. The deposition was carried out at both room temperature (RT) and 673 K and the deposited film thickness was fixed to 30 nm. Before the deposition, the silicon wafers were cleaned in sequence with acetone, isopropyl alcohol, and deionized water in the ultrasonic cleaner for 15 min each.

For measuring W film resistivity, a four-point probe (JANDEL ENG.) was used. The surface roughness of the deposited W film was investigated with atomic force microscopy (AFM, PSIA XE100) using the non-contact-mode as the operation mode. The crystal structure and

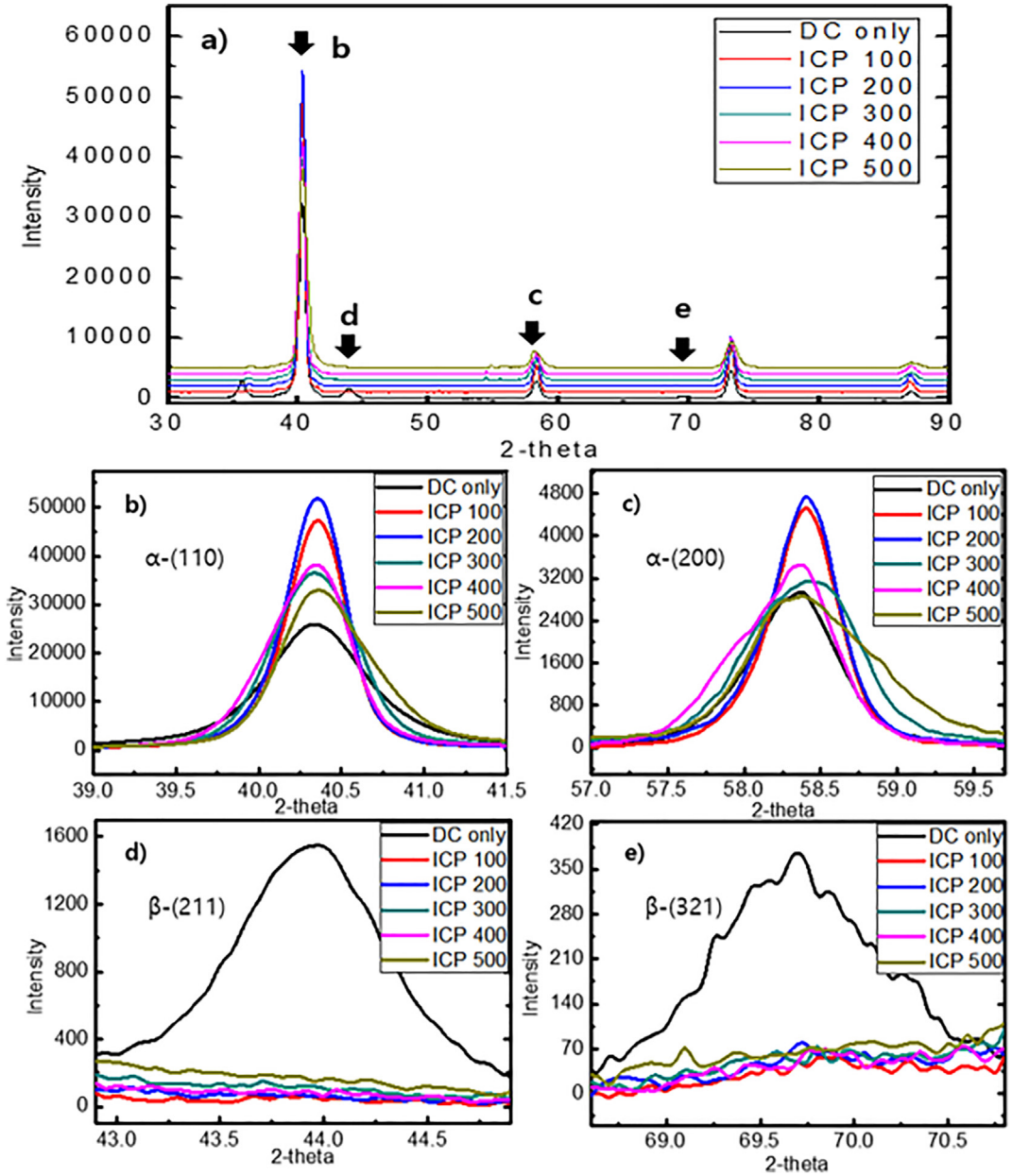

Fig. 5. XRD data of (a) W thin film and the XRD peaks of (b) α-(110), (c) α-(200), (d) β-(211), and (e) β-(321) as a function of ICP power from 0 to 500 W at RT.

grain size were investigated using X-ray diffraction (XRD, Rigaku Corporation MXD10, Cu target with 9 kW, Configuration with 0.3~1°). The chemical binding states of the deposited W film were investigated using X-ray photoelectron spectroscopy (XPS, ESCA2000, VG Microtech Inc.). As the XPS source type, Mg Kα was used and the binding energy measured by XPS was calibrated using carbon 1 s at 284.5 eV. The sample was etched by Ar ion beam for 300 s and the bias current was fixed at 20 μm.

3. Results and discussion

The deposition rate of W thin film as a function of ICP power for the ICP assisted DC magnetron sputtering has been investigated and the results are shown in Fig. 2. Ar operating pressure was maintained at 2.0 Pa and the DC power to the magnetron was kept at 500 W while varying the 13.56 MHz RF power to ICP source from 0 to 500 W. The substrate was maintained at RT or heated to 673 K using a substrate heater. The substrate was SiO_2 (20 mm × 20 mm) and the thickness of the W thin film was kept at 30 nm. As shown in Fig. 2, for both RT and 673 K, the addition and increase of ICP power from 0 to 500 W during the deposition of W thin film increased the deposition rate from 62 to 71 nm/min for RT and from 67 to 80 nm/min for 673 K. Therefore, the addition of ICP power increased the deposition rate and the deposition rate was higher at the higher substrate temperature.

Fig. 3 shows the voltage and current of the DC magnetron sputter magnetron power as a function of ICP power (from 0 to 500 W) while maintaining the DC magnetron power of 500 W at 2.0 Pa Ar for different substrate temperatures of RT and 673 K. The addition and increase of ICP power to 500 W while maintaining the DC magnetron power at 500 W increased the current almost linearly from 1.32 to 1.52–1.57 A while decreasing the voltage also almost linearly from 392 to 332–342 V. The increase of current to the DC magnetron is related to the increased ion density near the magnetron surface and, the decrease of DC voltage is due to the constant 500 W applied to the DC magnetron. The increased deposition rate observed in Fig. 2 with the addition and increase of the ICP power is due to the increased sputtered atom

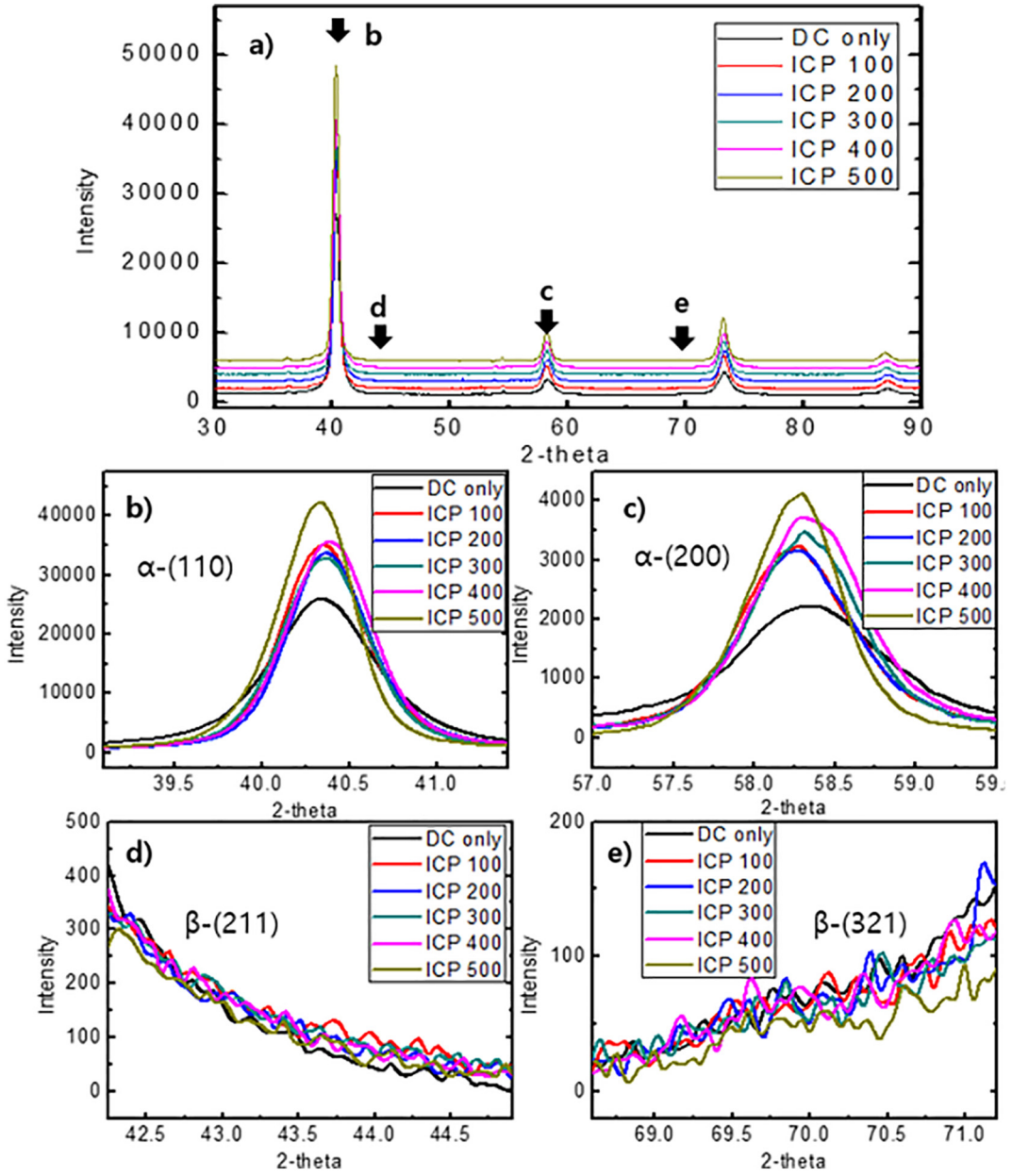

Fig. 6. XRD data of (a) W thin film and the XRD peaks of (b) α-(110), (c) α-(200), (d) β-(211), and (e) β-(321) as a function of ICP power from 0 to 500 W at 673 K.

flux by the increased Ar^+ ion density near the magnetron surface while the Ar^+ ion energy to the W target, which is related to the target voltage, is not significantly decreased. In addition, at the higher substrate temperature of 673 K, a little higher magnetron current was observed compared to RT, and, it is believed that the higher deposition rate observed at the higher substrate temperature [30] is partially related to the higher magnetron current observed at higher substrate temperature. (In fact, currently we do not know the exact reason why the magnetron current was increased and the deposition rate was increased at the higher substrate temperature; it might be related to the increased secondary electron emission from the substrate surface at the higher substrate temperature or might be related to the removal of residual water vapor in the chamber which absorbs electrons in the plasma by unintentional chamber baking during the substrate heating.)

The resistivity of 30 nm thick W thin film deposited by the ICP assisted DC magnetron sputtering has been investigated as a function of ICP power for two different substrate temperatures (RT and 673 K) and the results are shown in Fig. 4. As shown in Fig. 4, the addition of the ICP power (100–500 W) during the DC magnetron sputtering significantly decreased the resistivity of W thin film from 80 to ~ 30 μΩ-cm for RT and from 50 to ~ 20 μΩ-cm for 673 K. Also, in the case of RT, the resistivity was slightly increased (from 26 to 30 μΩ-cm) with the increase of ICP power from 200 to 500 W while the resistivity was continuously decreased (from 22 to 18 μΩ-cm) with the increase of ICP power from 100 to 500 W for 673 K. Therefore, the resistivity of 30 nm thick W thin film deposited by DC magnetron sputtering was the lower with ICP power assistance and at the higher substrate temperature.

To investigate the reason for the lower W resistivity with the ICP power assistance and at the higher substrate temperature, the variation of W crystal structure with different ICP powers was investigated by using XRD and the results are shown in Figs. 5 and 6 for different substrate temperatures of RT and 673 K, respectively: (a) XRD data of W thin film and the XRD peaks of (b) α-(110), (c) α-(200), (d) β-(211), and (e) β-(321) as a function of ICP power from 0 to 500 W. As shown in Fig. 5(a) and 6(a), α phase W peaks vs. 2θ related to the BCC structure are observed at 40.3° for (100) peak, 58.3° for (200) peak, 73.3° for

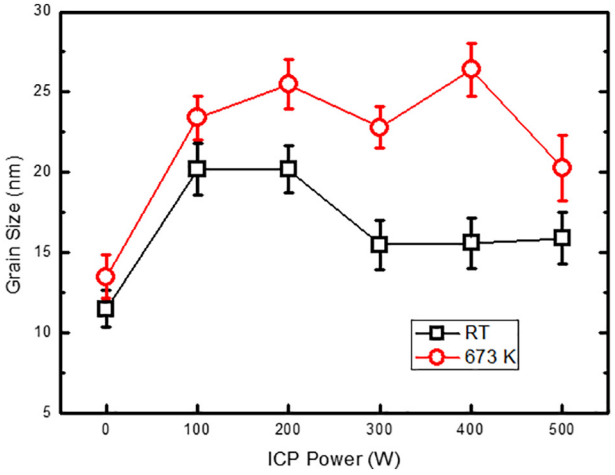

Fig. 7. Average grain size of W thin film estimated by Williamson-Hall Methods [18] using XRD data in Figs. 5 and 6 for RT and 673 K, respectively.

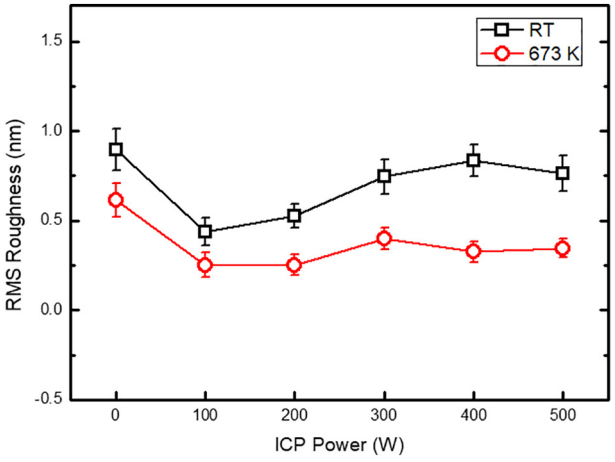

Fig. 8. RMS roughness of deposited W film measured as a function of ICP power for different substrate temperatures of RT and 673 K.

(211) peak, and 87° for (220) peak while β phase W peaks vs. 2θ related to the A-15 structure are observed at 35.7° for (200) peak, 44° for (211) peak, 66.8° for (320) peak, and 69.7° for (321) peak [3,31]. As shown in Fig. 5 (b) ~(e), for RT, the W thin film deposited with DC magnetron power showed β phase W peaks having A-15 structure in addition to α phase W peaks having BCC structure and, with the increase of ICP power up to 200 W, the β phase W peaks were removed and α-W peaks were increased. However, the further increase of ICP power to 500 W slightly decreased the α phase W peaks. In the case of 673 K, as shown in Fig. 6 (b) ~(e), the W thin film deposited with DC magnetron power only did not show β phase W peaks and the increase of ICP power up to 500 W increased α phase W peaks continuously. It is known that the β phase W has a higher resistivity (180–220 × μΩ-cm) compared to that of α phase W (24–50 × μΩ-cm), therefore, the W thin films with more α phase W crystals tend to show lower resistivity while those with more β phase W crystals tend to show higher resistivity. It is believed that the decrease of W resistivity at the higher substrate temperature of 673 K and with the assistance of ICP is observed in Fig. 4 partially related to the decrease of β phase W crystals and the increase of α phase W crystals in the film [32]. Also, the slight increase of resistivity with the increase of ICP power higher than 200 W for RT could be also related to the decreased α phase W crystals observed in Fig. 5 (b) and (c). In fact, the change of β phase W to α phase W in various deposition conditions of W thin film has been also observed by previous researchers; where, β phase W was observed at the film thickness lower than 7 nm [32,33], β

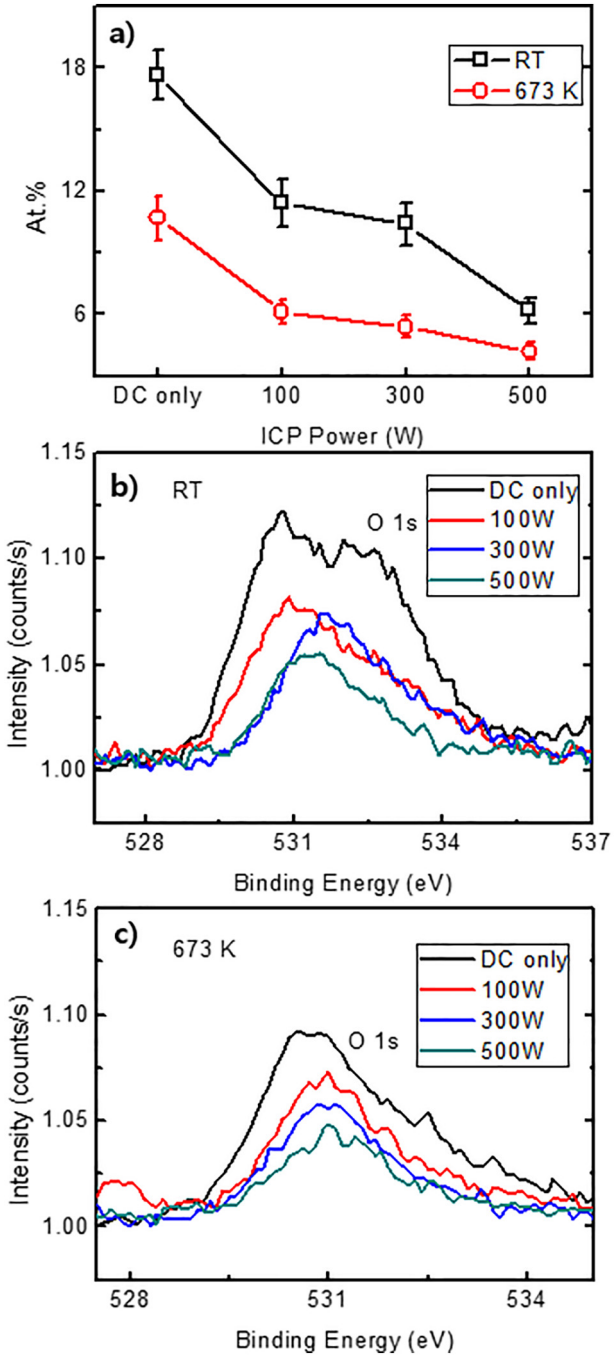

Fig. 9. (a) Relative oxygen content at the surface of W thin films prepared at substrate temperature of RT and 673 K as a function of the ICP power. O1s XPS spectra at (b) room temperature and (c) 673 K.

phase W changed to α phase W at higher substrate temperatures [3,34], and the tensile stress in the film showed β phase W while the compressively stressed film showed α phase W [35].

The average grain size of W thin film was estimated by Williamson-Hall Methods [36] using XRD data in Figs. 5 and 6 and the results are shown in Fig. 7. As shown in Fig. 7, for DC magnetron sputtering only, the grain sizes of the W thin films were ~11.5 nm and ~13.5 nm for RT and 673 K, respectively, and the addition of ICP power to the DC magnetron sputtering generally increased the average grain size to ~17.5 nm and ~23.7 nm for RT and 673 K, respectively, even though the increase of ICP power from 100 to 500 W did not change the grain size noticeably. The increased W grain size by the addition of ICP power

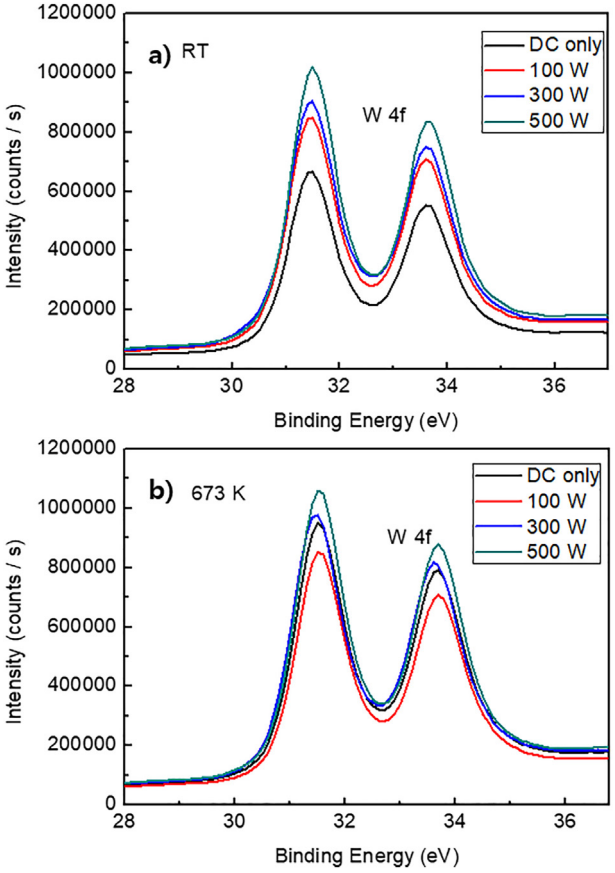

Fig. 10. W4f XPS spectra at (a) RT and (b) 673 K.

is believed to be related to the increased ion flux to the substrate which increases the mobility of the adatoms on the substrate during the grain growth [37,38]. The larger grain size by the addition of ICP power and by using higher substrate temperature decreases the grain boundary scattering of electron, therefore, lowers the resistivity.

Fig. 8 shows the RMS (root mean square) roughness of 30 nm thick W thin film surface measured using AFM with the scan size of 5 μm × 5 μm as a function of ICP power for two different substrate temperatures of RT and 673 K. As shown in Fig. 8, the surface roughness was lower for the higher substrate temperature and the addition of ICP power up to 100–200 W decreased the surface roughness (for RT, the use of DC only shows 0.89 nm of surface roughness but, after the addition of 100 W ICP, the surface roughness decreases to 0.44 nm, and for 673 K, DC only shows 0.62 nm and, after 100 W ICP, 0.25 nm), however, the further increase of ICP power increased the surface roughness slightly. The use of high substrate temperature and the addition of small ICP power increase the atomic surface mobility, therefore, the surface roughness can be decreased. However, the increase of surface roughness at the higher ICP power is believed to be related to the increased the deposition rate as investigated by other research [39]. Lower surface roughness decreases the electron scattering on the surface [14], therefore, the lower resistivity of the W thin film observed after the addition of ICP and with the higher substrate temperature in Fig. 4 is believed to be also partially related to the lower surface roughness in addition to the increased grain size and increased α phase W crystals.

Oxygen content in the deposited W thin film was also investigated using XPS. In general, after the W thin film deposition, the W thin film surface is oxidized at the atmosphere and forms W_3O or WO_3 which has A-15 structure [40]. Therefore, to remove the surface oxide formed during the air exposure, the W thin film surface was sputtered for 5 min using Ar in the XPS chamber and the oxygen percentage in the W thin film was investigated and the results are shown in Fig. 9 as a function of ICP power for two different substrate temperatures of RT and 673 K. The oxygen percentage was decreased continuously from 17.6 to 6.2% for RT and from 10.7 to 4.2% for 673 K by addition and increasing the ICP power from 0 to 500 W. The increased W atom/ion flux at the higher substrate temperature and higher ICP power as shown in Fig. 2 decreases the relative flux ratio of O/W, therefore, the oxygen content in the deposited W film can be decreased. In addition, for the higher substrate temperature, the oxygen percentage in the deposited film could be decreased by the decrease of the residual water vapor in the chamber by unintentional chamber baking even though the change of water vapor pressure at a higher substrate temperature was not measured. And, for the higher ICP power, the oxygen percentage in the deposited film can be also decreased by the preferential removal of adsorbed oxygen impurity by the enhanced ion bombardment at the higher ion flux to the substrate. The lower oxygen percentage obtained with higher substrate temperature and with the addition of ICP power can also decrease the W resistivity by lowering the electron scattering. (In Fig. 10 (a) and (b), XPS spectra of W 4f spectra for RT and 673 K are also shown, respectively. XPS peaks at 31.5 eV and 33.6 eV confirm the presence of metallic W (zero oxidation state)). Therefore, it is believed that, not only by the increased grain size, increased α phase W crystals, and decreased surface roughness, the decreased oxygen content in the W thin film affected the decreased the resistivity of the W thin film by using high substrate temperature and by the ICP assistance.

4. Conclusion

In this study, 30 nm thick W thin film was deposited using ICP assisted DC magnetron sputtering and the effect of ICP located near the DC magnetron sputtering source on the W thin film characteristics was investigated for two substrate temperatures of RT and 673 K. The addition of ICP during the DC magnetron sputtering increased the plasma density and decreased the voltage to the DC magnetron, therefore, the ion flux to the substrate was increased in addition to the increased deposition rate. The increased ion flux to the substrate decreased the oxygen content in the W thin film for the ICP power up to 500 W and also increased the grain size, decreased the surface roughness, and increased the α phase W crystals in the W thin film for the ICP power up to ~ 200 W. Similar effects such as increased grain size, lower oxygen content in the film, lower surface roughness, and more α phase W crystals could be obtained by increasing the substrate temperature. As a results, significantly lower W thin film resistivity could be obtained by the addition of ICP to the DC magnetron sputtering and by using high substrate temperature, and which could give a feasibility in replacing Cu to W as a next generation interconnect metal for the metal thickness lower than tens of nanometer.

Acknowledgment

This research was supported by the MOTIE (Ministry of Trade, Industry & Energy (10067827)) and Development of core-technology and components in organic electronics for ICT convergence support program for the development of the future display device.

Also, this research was supported by the Nano Material Technology Development Program through the National Research Foundation, South Korea (NRF), funded by the Ministry of Education, Science, and Technology (2016M3A7B4910429).

References

[1] Q.T. Jiang, M.H. Tsai, R.H. Havemanna, Line width dependence of copper resistivity, Proceed. IEEE Int. Interconnect Technol. Conf. (2001) 227–229, https://doi.org/10.1109/IITC.2001.930068.

[2] D. Choi, C.S. Kim, D. Naveh, S. Chung, A.P. Warren, N.T. Nuhfer, M.F. Toney, K.R. Coffey, K. Barmak, Electron mean free path of tungsten and the electrical resistivity of epitaxial (110) tungsten films, Phys. Rev. B 86 (2012) 045432, , https://

doi.org/10.1103/PhysRevB.86.045432.
[3] D. Choi, B. Wang, S. Chung, X. Liu, A. Darbal, A. Wise, Noel T. Nuhfer, K. Barmak, Phase, grain structure, stress, and resistivity of sputter-deposited tungsten films, J. Vacuum Sci. Technol. A 29 (2011) 051512, https://doi.org/10.1116/1.3622619.
[4] F. Chen, D. Gardner, Influence of line dimensions on the resistance of Cu interconnections, IEEE Electron Device Lett. 19 (1998) 508, https://doi.org/10.1109/55.735762.
[5] T. Sun, B. Yao, A.P. Warren, V. Kumar, S. Roberts, K. Barmak, K.R. Coffey, Classical size effect in oxide-encapsulated Cu thin films: Impact of grain boundaries versus surfaces on resistivity, J. Vacuum Sci. Technol. A 26 (2008) 605, https://doi.org/10.1116/1.2938395.
[6] T. Sun, B. Yao, A.P. Warren, K. Barmak, M.F. Toney, R.E. Peale, K.R. Coffey, Dominant role of grain boundary scattering in the resistivity of nanometric Cu films, Phys. Rev. B 79 (2009) 041402, , https://doi.org/10.1103/PhysRevB.79.041402.
[7] T. Sun, B. Yao, A.P. Warren, K. Barmak, M.F. Toney, R.E. Peale, K.R. Coffey, Surface and grain-boundary scattering in nanometric Cu films, Phys. Rev. B 81 (2010) 155454, https://doi.org/10.1103/PhysRevB.81.155454.
[8] J.R. Lloyd, M.W. Lane, E.G. Liniger, C.K. Hu, T.M. Shaw, R. Rosenberg, Electromigration and adhesion, IEEE Trans. Device Mater. Reliab. 5 (2005) 113–118, https://doi.org/10.1109/TDMR.2005.846308.
[9] J.W. McPherson, Reliability challenges for 45 nm and beyond, 2006 43rd ACM/IEEE Design Automation Conf, 2006, pp. 176–181, , https://doi.org/10.1145/1146909.1146959.
[10] J.H.-C. Chen, S.S.-C. Fan, T.E. Standaert, T.A. Spooner, V. Paruchuri, A study of tungsten metallization for the advanced BEOL interconnections, in: S.E. Schulz (Ed.), 2015 Advance Metallization Conference Proceedings, 2015 http://nbn-resolving.de/urn:nbn:de:bsz:ch1-qucosa-207035.
[11] D. Choi, The electron scattering at grain boundaries in tungsten films, Microelectron. Eng. 122 (2014) 5–8, https://doi.org/10.1016/j.mee.2014.03.012.
[12] J.R. Lloyd, J. Clemens, R. Snede, Copper metallization reliability, Microelectron. Reliab. 39 (1999) 1595–1602, https://doi.org/10.1016/S0026-2714(99)00177-8.
[13] C.S. Hau-Riege, An introduction to Cu electromigration, Microelectron. Reliab. 44 (2004) 195–205, https://doi.org/10.1016/j.microrel.2003.10.020.
[14] S.M. Rossnagel, T.S. Kuan, Alteration of Cu conductivity in the size effect regime, J. Vacuum Sci. Technol. B 22 (2004) 240, https://doi.org/10.1116/1.1642639.
[15] H.H. Jeon, V.P. Verma, K.S. Noh, D.H. Kim, W.B. Choi, M.H. Jeon, Fabrication and characteristics of zinc oxide- and gallium doped zinc oxide thin film transistor using radio frequency magnetron sputtering at room temperature, J. Kor. Vac. Soc. 16 (5) (2007) 359–365, https://doi.org/10.5757/JKVS.2007.16.5.359.
[16] M.Y. Hur, S. Oh, H.J. Kim, H.J. Lee, Numerical analysis of the incident ion energy and angle distribution in the DC magnetron sputtering for the variation of gas pressure, Appl. Sci. Converg. Technol. 27 (2018) 19–22, https://doi.org/10.5757/ASCT.2018.27.1.19.
[17] J.M. Schneider, S. Rohde, W.D. Sproul, A. Matthews, Recent developments in plasma assisted physical vapour deposition, J. Phys. D 33 (2000) 173, https://doi.org/10.1088/0022-3727/33/18/201.
[18] A. Palmero, H. Rudolph, F.H.P.M. Habraken, One-dimensional analysis of the rate of plasma-assisted sputter deposition, J. Appl. Phys. 101 (2007) 083307, , https://doi.org/10.1063/1.2720257.
[19] S.J. Jung, Y.H. Han, J.J. Lee, Deposition of Al doped ZnO films using ICP-assisted sputtering on the plastic substrate, J. Kor. Inst. Surf. Eng. 39 (3) (2006) 98–104 http://www.dbpia.co.kr/Journal/ArticleDetail/NODE01005207.
[20] S. Lee, J. Yang, S. Jung, D.-G. Kim, E. Byeon, Collisional ion energy transfer model for understanding wrinkles on poly (dimethylsiloxane) surfaces after oxygen ion beam irradiations, Appl. Sci. Converg. Technol. 27 (2018) 130–134, https://doi.org/10.5757/ASCT.2018.27.6.130.
[21] J.W. Lim, H.S. Park, T.H. Park, J.J. Lee, J.H. Joo, Mechanical properties of titanium nitride coatings deposited by inductively coupled plasma assisted direct current magnetron sputtering, J. Vac. Sci. Technol. A 18 (2000) 524, https://doi.org/10.1116/1.582219.
[22] B.H. Kim, J.H. Han, S.H. Kwon, Y.J. Yoon, Preparation of MoS2 nanopetals by RF magnetron sputtering and electron-beam irradiation, Appl. Sci. Converg. Technol. 27 (2018) 149–152, https://doi.org/10.5757/ASCT.2018.27.6.149.
[23] J. Pan, C. Leygraf, D. Thierry, A.M. Ektessabi, Corrosion resistance for biomaterial applications of TiO_2 films deposited on titanium and stainless steel by ion-beam-assisted sputtering, J. Biomed. Mater. Res. 35 (1997) 309–318, https://doi.org/10.1002/(SICI)1097-4636(19970605)35:3<309::AID-JBM5>3.0.CO;2-L.
[24] A.M. Ektessabi, Ion-beam-assisted sputter deposition of thin oxide films, Surf. Coat. Technol. 68–89 (1994) 208–216, https://doi.org/10.1016/0257-8972(94)90162-7.
[25] D.H. Kim, Y.G. Han, J.S. Cho, S.K. Koh, Low temperature deposition of ITO thin films by ion beam sputtering, Thin Solid Films 377-378 (2000) 81–86, https://doi.org/10.1016/S0040-6090(00)01388-2.
[26] Y. Huh, Y. Hwang, J. Kim, Study of driving and thermal stability of anode-type ion beam source by charge repulsion mechanism, Appl. Sci. Converg. Technol. 27 (2018) 47–51, https://doi.org/10.5757/ASCT.2018.27.3.47.
[27] C.H. Lee, T.H. Kim, S.M. Lee, J.W. Bae, K.N. Kim, G.Y. Yeom, Properties of IGZO film deposited by Ar/O_2 inductively coupled plasma assisted DC magnetron sputtering, Sci. Adv. Mater. 9 (2017) 1187–1192, https://doi.org/10.1166/sam.2017.2886.
[28] B.B. Sahu, J.G. Han, J.B. Kim, M. Kumar, S. Jin, M. Hori, Study of plasma properties for the low-temperature deposition of highly conductive aluminum doped ZnO film using ICP assisted DC magnetron sputtering, Plasma Process. Polym. 13 (2016) 134–146, https://doi.org/10.1002/ppap.201500094.
[29] I.H. Yang, Y.J. Lee, J.N. Jang, M. Hong, Study of the inductively coupled plasma assisted DC magnetron sputtering (ICPDMS) during ITO deposition, Thin Solid Films 517 (2009) 4165–4169, https://doi.org/10.1016/j.tsf.2009.02.032.
[30] E. Camacho-Espinosa, E. Rosendo, T. Díaz, A.I. Oliva, V. Rejon, J.L. Peña, Effects of temperature and deposition time on the RF-sputtered CdTe films preparation, Superf. Vacío 27 (1) (2014) 15–19 mexico mar. http://www.scielo.org.mx/scielo.php?pid=S1665352120140001000004&script=sci_arttext.
[31] M.J. O'Keefe, J.T. Grant, Phase transformation of sputter deposited tungsten thin films with A-15 structure, J. Appl. Phys. 79 (1996) 9134, https://doi.org/10.1063/1.362584.
[32] J.S. Lee, J.H. Cho, C.Y. You, Growth and characterization of α and β-phase tungsten films on various substrates, J. Vacuum Sci. Technol. A 34 (2016) 021502, , https://doi.org/10.1116/1.4936261.
[33] S.M. Rossnagel, I.C. Noyan, C. Cabral Jr., Phase transformation of thin sputter-deposited tungsten films at room temperature, J. Vac. Sci. Technol. B 20 (2002) 2047, https://doi.org/10.1116/1.1506905.
[34] P. Petroff, T.T. Sheng, A.K. Sinha, G.A. Rozgonyi, F.B. Alexander, Microstructure, growth, resistivity, and stresses in thin tungsten films deposited by rf sputtering, J. Appl. Phys. 44 (1973) 2545, https://doi.org/10.1063/1.1662611.
[35] T.J. Vink, W. Walrave, J.C.L. Daams, A.G. Dirks, M.A.J. Somers, K.J.A. Van der Aker, Stress, strain, and microstructure in thin tungsten films deposited by dc magnetron sputtering, J. Appl. Phys. 74 (1993) 988, https://doi.org/10.1063/1.354842.
[36] A.R. Stokes, A.J.C. Wilson, The diffraction of X rays by distorted crystal aggregates – I, Proc. Phys. Soc. 56 (1944) 174, https://doi.org/10.1088/0959-5309/56/3/303.
[37] X. Qi, C. Ren, T. Ma, Y. Wang, Cu films deposited by unbalanced magnetron sputtering enhanced by ICP and external magnetic field confinement, Plasma Sci. Technol. 10 (2008) 319, https://doi.org/10.1088/1009-0630/10/3/10.
[38] Y.S. Yoon, K.H. Kim, H.G. Jang, H.J. Jung, S.K. Koh, Characteristics of Cu thin films on a glass substrate by partially ionized beam deposition at room temperature, J. Vac. Sci. Technol. A 14 (1996) 2517, https://doi.org/10.1116/1.580012.
[39] P. Zhang, X. Zheng, S. Wu, J. Liu, De He, Kinetic Monte Carlo simulation of Cu thin film growth, Vacuum 72 (2004) 405–410, https://doi.org/10.1016/j.vacuum.2003.08.013.
[40] I.A. Weerasekera, S.I. Shah, D.V. Baxter, K.M. Unruh, Structure and stability of sputter deposited beta-tungsten thin films, Appl. Phys. Lett. 64 (1994) 3231, https://doi.org/10.1063/1.111318.